Controlled magnetic roughness in a multilayer that has been patterned using a nanosphere array

Sean Langridge,[1,*] L. A. Michez,[2,†] M. Ali,[2] C. H. Marrows,[2] B. J. Hickey,[2] T. R. Charlton,[3,‡] R. M. Dalgliesh,[1] M. Toohey,[4] E. W. Hill,[4] S. McFadzean,[5] and J. N. Chapman[5]

[1]*ISIS, Rutherford Appleton Laboratory, Chilton, OX11 0QX, United Kingdom*

[2]*School of Physics and Astronomy, E.C. Stoner Laboratory, University of Leeds, Leeds, LS2 9JT, United Kingdom*

[3]*Material Science Division, Argonne National Laboratory, Argonne, Illinois 60439, USA*

[4]*Department of Computer Science, University of Manchester, Manchester, M13 9PL, United Kingdom*

[5]*Department of Physics and Astronomy, University of Glasgow, Glasgow, G12 8QQ, United Kingdom*

(Received 25 November 2005; published 14 July 2006)

The micromagnetic structure of an antiferromagnetically exchange-coupled multilayer constrained by a periodic in-plane structure has been quantified using polarized-neutron reflectometry. The pattern was realized through nanosphere lithography. The fabrication of the patterned array introduces a significant deviation in the in-plane magnetization direction near to and at the surface of the heterostructure but does not significantly perturb the domain structure. The characteristic length scale of this magnetic roughening is shown to be driven by the feature size. The roughening is not observable by conventional magnetometry techniques but is confirmed by micromagnetic simulation. The combination of scattering techniques and numerical simulation provides a powerful tool to study the subtle interlayer and intralayer ordering in patterned magnetic heterostructures.

DOI: 10.1103/PhysRevB.74.014417 PACS number(s): 75.25.+z, 73.21.Ac

Magnetic heterostructures have undergone extensive research over the past two decades both as a way of artificially testing fundamental physical interactions and for their technological applications. For example, this research has resulted in the discovery of interlayer coupling,[1,2] giant-magnetoresistance[3] (GMR), and more recently, effects associated with the properties of spin-polarized currents,[4,5]: namely, spin electronics. Moreover, high storage densities or high current densities for the spin torque switching of nanopillars,[6] etc., requires systems that are nanoscaled in all three dimensions. While significant insight can be gained from a single device it is also important to understand their behavior when placed in large-area arrays. This has attracted recent interest ranging from artificial frustrated magnetism[7] and digital computation[8] to candidates for high-density recording media.[9] Interfacial effects or interfeature coupling resulting in localized deviations in the magnetization direction will significantly affect electron transport: a significant challenge is then to unravel the interplay between a controlled structure and the competing balance of magnetic interactions. To this purpose neutron scattering,[10] polarized-neutron reflectivity[11] (PNR), and x-ray resonant magnetic scattering[12] (XRMS) are the techniques of choice, providing statistically significant sampling over large areas. Conventional magnetometry and imaging are not well suited to studying these interfacial and buried spins, either lacking sensitivity or the ability to probe the internal chemical and magnetic structure.

Here we show, through the use of off-specular neutron reflectometry, that for samples with a controlled roughness and in-plane morphology, local deviations in the magnetization direction are generated, but the domain structure remains unchanged. These results are further substantiated by micromagnetic simulations.

Deviations in the magnetization directions and uncompensated spins arising from structural disorder give rise to the diffuse scattering of x rays and neutrons even in samples which, according to conventional magnetometry, are saturated. This magnetic morphology, which can be different from the structural one, has come to be known as "magnetic roughness," and there are now several experiments in continuous systems which reveal the subtle interplay between the structural and magnetic aspects of the disorder.[13–17] Given that the magnetization is a vector quantity we can envisage several different mechanisms for its disorder (cf. a structural, scalar surface). Broadly, these may be classified as a nonuniform distribution of magnetization direction—i.e., a domain distribution[18]—or a structurally rough interface which will have a magnetic surface that deviates from an ideal plane and is said to possess *magnetic roughness*. Here we consider the additional complexity of a system that is structurally patterned on a comparable length scale to typical magnetic domain sizes. In this latter case one needs to consider in more detail the balance between the competing magnetic interactions between the patterned structures. The dipolar coupling and its competition with the exchange and the Zeeman interactions may lead to ordering on very different length scales ranging from short-range magnetic roughness to long-range magnetic stripe order. The off-specular PNR technique provides access to all of these phenomena and complements surface-sensitive real-space imaging techniques such as photoemission electron microscopy (PEEM).[19]

The antiferromagnetic (AFM) coupling and domain structure in smooth superlattices is well understood and has been extensively characterized with PNR (Ref. 20) and XRMS (Ref. 21) techniques. In summary, they are characterized by micron-size magnetic domains at remanence that are for reasonably strongly coupled systems, vertically correlated, and in which there is no evidence of magnetic roughness. To introduce a well-defined in-plane periodicity we have used 0.22-μm-diam polystyrene (PS) spheres[22,23] to produce a mask for the deposition of Au nanodots to act as a template for the deposition of AFM-coupled Co/Ru multilayers. The

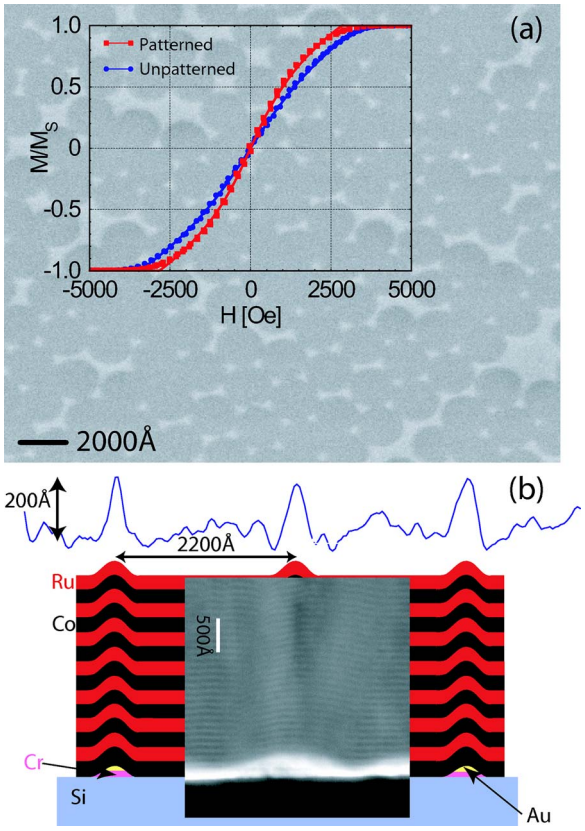

FIG. 1. (Color online) (a) A scanning electron micrograph (SEM) of the completed sample. The sphere size is 2200 Å, and some degree of hexagonal close packing is clearly visible. The inset shows the normalized magnetization curves for the unpatterned and patterned samples. The solid lines are fits as described in the text. (b) A schematic of the multilayer system. The line shows the structural surface profile extracted from the SEM. The inset shows an XTEM image of the multilayer structure, the topography and the substrate.

nanosphere lithography was carried out by spin coating polystyrene spheres suspended in water onto 25 mm × 20 mm pieces cut from a (001)-oriented Si wafer that had just been subjected to a pirahna etch (a combination of H_2O_2 and HNO_3). A 50-Å Cr layer followed by a 150-Å layer of Au was then evaporated over the spheres. The spheres were subsequently removed with an acetone wash. An AFM-coupled multilayer was deposited on top of the form $[Co(20\ Å)/Ru(18\ Å)]_{50}$. The multilayers were deposited by dc magnetron sputtering. A scanning electron micrograph (SEM) and cross-sectional transmission electron micrograph (XTEM) of the completed sample are shown in Fig. 1. The multilayer structures were prepared with Ru spacer thicknesses corresponding to the second peak of the AFM coupling oscillation.[2] The surface consists of 2200-Å-sized, circular regions surrounded by raised regions. XTEM shows that the multilayer structure follows smoothly the dots [see Fig. 1(b)]. An analysis of the x-ray reflectometry from these samples reveals that the patterning process increases the structural rms roughness from 3±0.4 Å up to 6±0.5 Å but still retains the vertically coherent structure. The diffuse

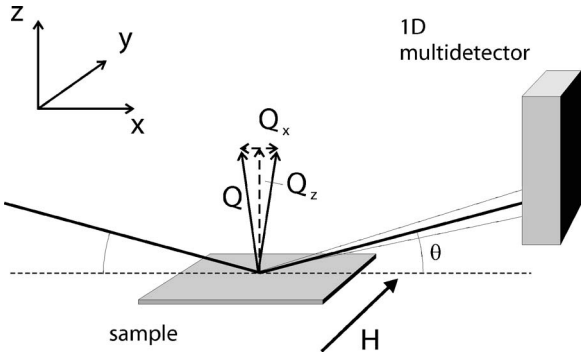

FIG. 2. The experimental geometry used. The incident beam of neutrons from the left is reflected by the sample and detected on the 1D detector to the right. Intensity is integrated over Q_y. Typical values for the angle θ are ~1°. Note that in principle the geometry is not limited by the sample horizon, in contradistinction to the x-ray case, and the detector may extend below the sample plane to collect data in transmission as well as in reflection. The magnetic field **H** is applied perpendicular to the scattering plane.

x-ray scattering gives $\xi_s \sim 250$ Å and 400 Å for the structural in-plane and out-of-plane correlation lengths, respectively. This compares to $\xi_s \sim 250$ Å and 580 Å, respectively, for the unpatterned system. Moreover, the patterning results in an increase in the coercive field from 40 to 50 Oe, presumably as a result of increased domain wall pinning centers from the patterning process. Analyzing the magnetization[24] curves gives a bilinear coupling of $-0.62\ mJ\ m^{-2}$ and $-0.58\ mJ\ m^{-2}$ for the unpatterned and patterned films respectively. The much weaker biquadratic coupling increases from $-0.05\ mJ\ m^{-2}$ to $-0.07\ mJ\ m^{-2}$. This small change in coupling is presumably due to the increased structural roughness and an increase in thickness fluctuations caused by the patterning process.[25]

Our main measurement technique was PNR, carried out at the CRISP reflectometer at the ISIS facility.[26] The instrument was operated in both an unpolarized and polarized mode in order to maximize the available flux at the sample and to provide additional information on the magnetic structure, respectively. The reflected neutrons were detected with a one-dimensional ^{3}He detector. The combination of the time-of-flight technique and the multidetector ensures that both the parallel (Q_z) and perpendicular (Q_x) (to the surface normal) components of the neutron wave vector are obtained in a single measurement. Typical acquisition times are of the order of 2 h for an entire reciprocal-space map. All measurements were performed at room temperature.

The measurement geometry used in the experiments is shown in Fig. 2. The one-dimensional (1D) multidetector was set up in the scattering plane, so that the transverse component of the wave-vector transfer Q_x is in the scattering plane and perpendicular to the applied field. Hence the neutron intensity is integrated over Q_y. Representative (unpolarized) data are presented in Fig. 3 and show the reciprocal-space map for the unpatterned (a) and patterned (b) samples at the coercive field, H_c=40 Oe and 50 Oe, respectively. Concentrating on the upper panel: for Q_z=0.165 $Å^{-1}$, the first-order Bragg peak (n=1) is visible. This arises from

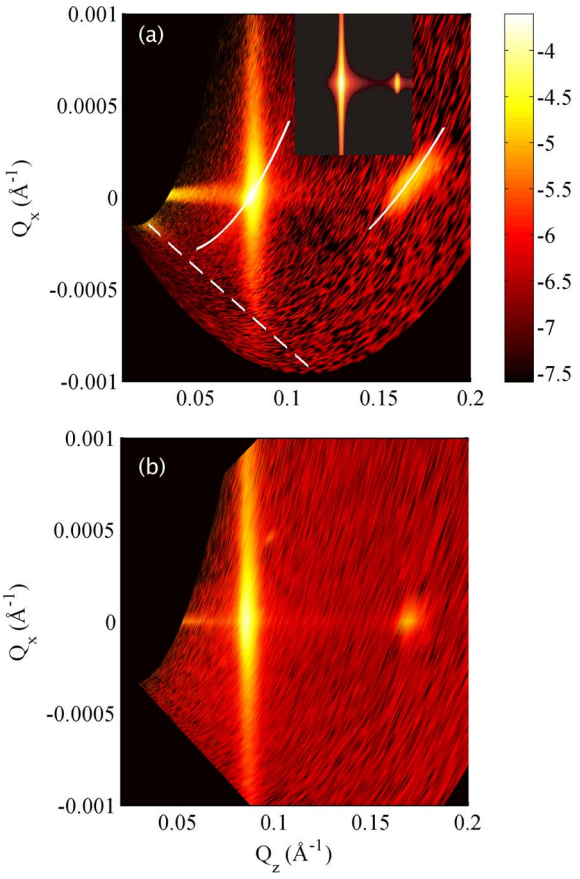

FIG. 3. (Color online) The reciprocal-space map for the unpatterned (a) and patterned (b) structures at the coercive field. The colorbar indicates the logarithm of the measured intensity. The inset [panel (a)] shows the calculated reciprocal space surface for the AFM domain structure described by Eq. (5) over the same range of reciprocal space. Note that the range of the experimental data is restricted by the kinematical limits of the measurement.

the structural periodicity of the multilayer and also conveys information on any magnetic contribution of the same periodicity—i.e., ferromagnetic (FM) ordering between neighboring bilayers in the multilayer. At the coercive field the magnetic contribution at this wave vector is zero—i.e., no net magnetization. There is no evidence of diffuse scattering which would be indicative of a large degree of correlated structural (magnetic) roughness. At half of this wave vector, Q_z=0.083 Å^{-1}, a Bragg peak $\left(n=\frac{1}{2}\right)$ is visible that corresponds to AFM ordering and hence this peak is purely magnetic in origin. Away from the specular ridge significant diffuse scattering is visible, indicative of a vertically correlated in-plane AFM domain structure through the entire multilayer [≈2000 Å (Ref.18)] structure. The anomalies in the peak shape at the two Bragg peaks are due to a generalized Yoneda effect[27] in which the scattered neutron wave vector satisfies the Bragg condition.[28] The dashed line in the top panel indicates the expected Yoneda scattering. The solid loci indicate the reciprocal-space coordinates which satisfy this condition—i.e.,

$$\theta = \frac{Q_z}{2Q} - \frac{Q_x}{Q_z}, \tag{1}$$

where $Q=2\pi/\lambda$ for the neutron wavelength λ satisfying the Bragg condition. The loci are in good agreement with the experimental observations. The scattering from the patterned system (lower panel) at the coercive field shows a similar AFM domain distribution but does not show the generalized Yoneda features due to the additional structural roughening induced by the patterning process.

In order to quantitatively analyze the off-specular neutron scatter it is necessary to develop a theoretical framework for diffuse scatter in systems in which both structural and magnetic disorder is present. We include structural fluctuations by following a slightly simplified version of the model of Sinha *et al.*,[29] where the height of the surface is treated as a Gaussian random variable $z(\mathbf{r})$ and is characterized by a correlation function

$$C(|\mathbf{r}-\mathbf{r}'|) = \langle z(\mathbf{r})z(\mathbf{r}')\rangle = \sigma_s^2 \exp(-|\mathbf{r}-\mathbf{r}'|/\xi_s), \tag{2}$$

where σ_s is the rms roughness, the width of the Gaussian distribution of z, and ξ_s is the in-plane structural correlation length.

It is necessary to parametrize any magnetic domain structure in a similar manner: we assume that the perpendicular component of $\mathbf{m}(\mathbf{r})$ is zero due to the shape anisotropy of the film, so the vector $\mathbf{r}$ is now restricted to only two dimensions, and that $|\mathbf{m}|=m_{sat}$ is constant inside the magnetic layer—i.e., the magnetic inhomogeneities are solely directional variations within the x-y plane; it is then convenient to parametrize in terms of an in-plane angle $\phi(\mathbf{r})$, giving

$$\mathbf{m}(\mathbf{r}) = m_{sat}(\sin\phi(\mathbf{r}), \cos\phi(\mathbf{x}), 0), \tag{3}$$

measuring the angle relative to the applied field. Again we treat ϕ as a Gaussian random variable,[30] and write a magnetic correlation function

$$M(|\mathbf{r}-\mathbf{r}'|) = \langle \phi(\mathbf{r})\phi(\mathbf{r}')\rangle = \sigma_m^2 \exp(-|\mathbf{r}-\mathbf{r}'|/\xi_m), \tag{4}$$

with σ_m being the rms deviation of ϕ from the field direction the width of the Gaussian distribution in ϕ and ξ_m the magnetic correlation length. This yields, for example, the global magnetization in the field direction as $m_0\exp(-\sigma_m/2)$. For scattering which is sufficiently weak (such as at the reasonably large scattering wave vectors $\mathbf{Q}$ employed in our measurements) we are able to make use of the more tractable Born approximation (BA) as opposed to the distorted-wave Born approximation[31] which includes dynamical scattering effects. This approach then allows one to readily characterize the magnetic order in a computationally efficient manner. Here we can separate the scattering into the long-range-

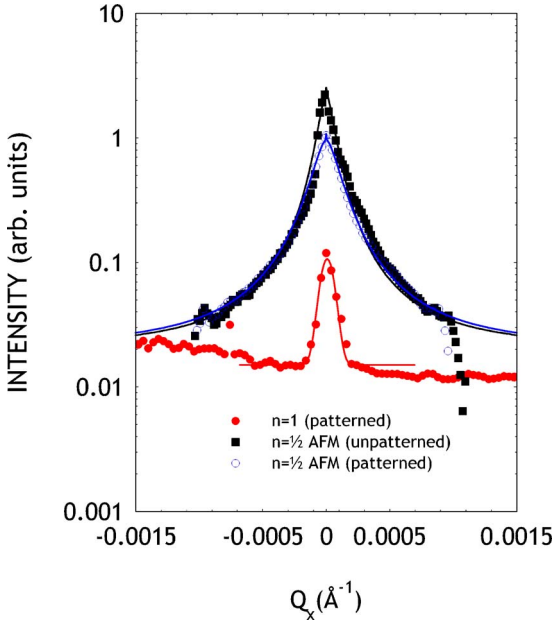

FIG. 4. (Color online) Transverse cuts (Q_X) at the coercive field, normalized to the incident beam intensity, through the FM/structural ($n=1$) and AFM ($n=\frac{1}{2}$) Bragg peaks for the unpatterned and patterned samples. The solid lines are fits to the model described in the text.

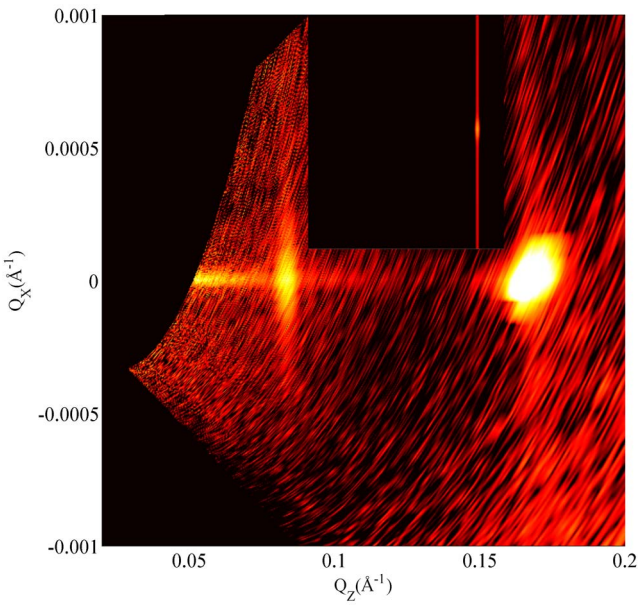

FIG. 5. (Color online) Reciprocal space maps for the patterned system at an applied field, $H=4.7$ kOe. Weak vertically correlated AFM correlations are present along with a correlated magnetic roughness at the first order Bragg peak position; cf. Fig. 3. The inset shows the calculation for the scattering solely from the short-range disorder described in the text.

ordered structure (both magnetic and structural) which gives rise to specular scattering S_{spec} and to the three diffuse components within S_{diff} (Ref. 18):

$$S_{\text{diff}}(\mathbf{Q}) \propto \int d^2\mathbf{r} e^{i\mathbf{Q}\cdot\mathbf{r}}[s+m+sm], \tag{5}$$

where s arises from the structural roughness, m from the angular variation of the magnetization, and sm the interference between the two terms—i.e., the magnetic roughness. To quantify the domain structure we then apply the previously described formalism to the transverse cuts through the Bragg peaks as shown in Fig. 4. For the unpatterned sample, deposited onto a native oxide silicon substrate during the same growth run, the extracted domain size is 3.4 ± 0.5 μm. For the patterned system, the domain size extracted is 3.9 ± 0.5 μm. The domain size does not change significantly with patterning and is much larger than the pattern size. The magnetization direction is then coherent over $\sim$15 sphere diameters. This long-range magnetic order is not surprising given the smooth nature of the layers as revealed by the XTEM.

At the AFM ordering wave vector the scattering is entirely diffuse in nature for both samples, showing that the AFM domains are completely randomly oriented within the plane of the multilayer at the coercive field; i.e., the distribution of the domain magnetization direction can be characterized by an angular spread $\sigma_{\text{m}} \approx 2\pi$ rad. Moreover, the AFM domains are vertically correlated throughout the entire structure.

Through the application of a large magnetic field it is then possible to produce a single-domain state. For both our unpatterned and patterned samples in fields close to saturation, weak AFM correlations are still present. For the unpatterned sample there is no evidence of diffuse scattering at the FM ordering wave vector, while for the patterned sample, diffuse intensity was observed around the first-order Bragg peak as shown in Fig. 5. Through the application of a magnetic field we have almost suppressed the AFM domain structure (note that according to our magnetometry measurements the bulk sample is saturated at this field) but have generated weak diffuse scattering at the first-order Bragg peak position. The applied magnetic field dependence of this scattering signifies magnetization which is not aligned with the bulk magnetization of the sample: this is a signature of magnetic roughness. Furthermore, the sensitivity to the applied field implies that this noncollinear magnetization is not pinned but is free to rotate.

By now using an incident polarized beam we can take advantage of the spin dependence of the neutron scattering potential to isolate the magnetic contribution to the scattering. The transverse cuts through the first-order Bragg peak are shown in Fig. 6 for $H=4.7$ kOe for incident spin-up (-down) polarized neutrons as indicated by the circle (square) symbols. As the sample approaches saturation the neutron spin-dependent Bragg peak increases in intensity due to the FM contribution and additional diffuse scattering above the background level is apparent. Analyzing the diffuse scattering as shown in Fig. 6 yields a length scale for the magnetic roughness of $\xi_{sm} \leq 1900\pm500$ Å, roughly the sphere diameter. The width of the effective angular distribution of the magnetic moments at 4.7 kOe is characterized by $\sigma_{\text{m}} = 0.5\pm0.1$ rad. Surprisingly, the length scale of the magnetic

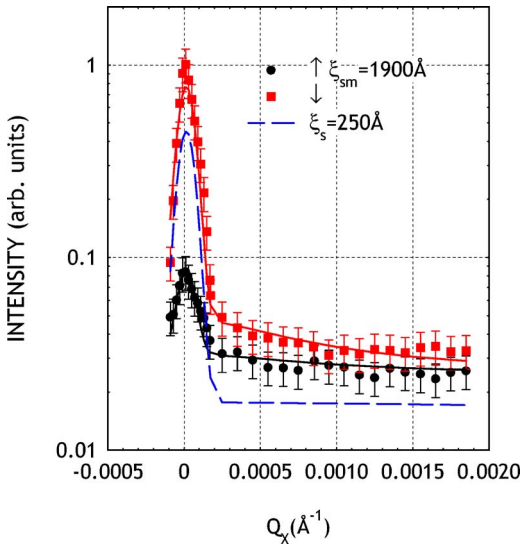

FIG. 6. (Color online) Transverse cuts (Q_z=0.165 Å^{-1}) through the FM/structural Bragg peak (Ref. 32) for incident neutron spin eigenvectors of up (down) as indicated by the circle (square) symbols. The solid lines are fits to the model described by Eq. (5). The dashed line is the scattering from a system with a length scale driven by the structural correlation length ($\xi_s \sim 250$ Å) for comparison and is offset for clarity.

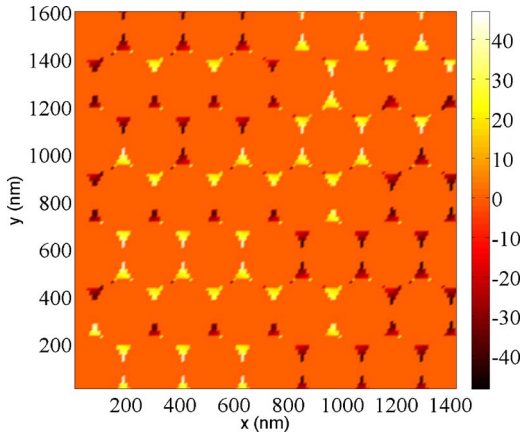

FIG. 7. (Color online) The micromagnetic simulation of the idealized surface region at 4.7 kOe applied in the $-ve$ x direction. The color scale refers to the angular variation (deg) in the x-y plane.

roughness is comparable to the size of the PS spheres; i.e., the patterning process determines the length scale over which the moments are coherent. At an applied field of 4.7 kOe the moments are still significantly misaligned with respect to the bulk magnetization and applied magnetic field. Conventional magnetometry indicates that for this field the sample is magnetically saturated (see Fig. 1) but clearly this is not the case. Conversely, for a pinned structure the magnetic roughness would not move in reciprocal space upon the application of a saturating magnetic field as is the case here. This leads us to conclude that the moments are approximately aligned with the bulk in a single-domain state.

To further understand the magnetic ordering introduced by the patterning process we have performed micromagnetic simulations[33] of the idealized system.[34] Using the bulk Co magnetization, exchange stiffness, and the coupling energies extracted from the hysteresis loop, it is possible to simulate the magnetic microstructure.

This simulated microstructure is complicated as it contains the behavior characteristic of a continuous AFM-coupled multilayer and a patterned structure (see Fig. 7). Close to the coercive field the essentially continuous region of the multilayer exhibits micron-sized magnetic domains. This is consistent with our neutron observation of comparable domain sizes in the patterned and unpatterned samples. In this field, the surface regions are then single-domain states which are AFM coupled to the bulk domain structure. This is the well-known effect of AFM coupling to stabilize domain structures as used in commercial recording media.[35] The patterned structure is therefore AFM coupled and vertically coherent with the bulk domain structure and as such has a similar, but weaker, neutron scattering profile and is not visible above the large bulk domain signal. As the field is increased the bulk domains increase in size and the moments focus around the applied field direction with a sizable FM component. For the surface-patterned regions it is now energetically more favorable to form Néel-type domain states within a given structure, which tends to break the in-place correlations even though the continuous bulk of the structure approached a single-domain state. It is this magnetic phase, near to the surface, with a correlation length given by the approximate patterning size, that is observed in our neutron measurement (Fig. 6) near to saturation. Moreover, the angular variation (Fig. 7) between the towers is $\sigma_m \approx \pm 0.44$ rad and so agrees with our neutron analysis. This variation is primarily in-plane and orthogonal to the applied field direction (y direction) due to the shape anisotropy. This result is analogous to studies on mesoscopic antidot arrays[36] which develop a nonuniform, micron-size, domain distribution. At true saturation all of the structure is aligned and no magnetic diffuse scattering would be visible in the neutron experiment. We now turn to the differing behavior from unpatterned systems. XRMS studies of *ferromagnetic* thin films and trilayers[17,37] show the structure-magnetism correlation length to be correlated with and longer than the structural correlation length (typically 1500 Å and 1000 Å, respectively). In such studies the surface structural disorder is controlled through deposition techniques and results in a length scale much shorter than the typical domain size. These types of measurements were significantly extended by Takeda *et al.*[38] to AFM-coupled Fe/Cr multilayers using PNR. No definitive conclusions or quantitative analysis were possible on the nature of the disorder (domain versus roughness); nor were there any differences observed between the different substrates used. In contrast to this, in our patterned systems the magnetic roughness length scale is driven by the feature size and not the grain size, which is typically of the order of 200 Å.[39] That the magnetic roughness exhibits a significantly longer correlation length scale is not surprising given that the grains are not isolated but are magnetically coupled. It is interesting to note that in perfect systems simulated numerous interesting magnetic phases are observed depending on the applied field direction. From our patterning process the physical template consists of a distribution of structural do-

mains which will mask out the predicted phases from our neutron measurements which is sampling over an area of $\approx 625\ \mathrm{mm}^2$.

To summarize, the patterning of an AFM-coupled multilayer generates a magnetic roughness on a length scale driven by the sphere size while the domain structure is essentially unperturbed. The experimental observations are in quantitative agreement with numerical simulations of the micromagnetic structure. The quantified magnetic roughness, generated by interfeature interactions, will significantly influence the transport of spin-polarized currents, particularly as the feature size is reduced as in the case of nanopillars and the interactions (dipolar, self Oersted field etc.) increase.

We thank the EPSRC (Grants Nos. EP/D002761/1 and EP/D000661/1) for financial support.

*Electronic address: s.langridge@rl.ac.uk; URL: http://www.isis.rl.ac.uk

†Present address: CRMCN-CNRS UPR 7251, Campus de Luminy, Case 913, 13288 Marseille Cedex 9, France.

‡Present address: Rutherford Appleton Laboratory, Chilton, OX11 0QX, United Kingdom.

[1] P. Grünberg, R. Schreiber, Y. Pang, M. B. Brodsky, and H. Sower, Phys. Rev. Lett. **57**, 2442 (1986).

[2] S. S. P. Parkin, N. More, and K. P. Roche, Phys. Rev. Lett. **64**, 2304 (1990).

[3] M. N. Baibich, J. M. Broto, A. Fert, F. Nguyen VanDau, F. Petroff, P. Etienne, B. Greuzet, A. Friederich, and J. Chazelas, Phys. Rev. Lett. **61**, 2472 (1988).

[4] G. Prinz, Science **282**, 5394 (1998); **283**, 330(E) (1999); J. Magn. Magn. Mater. **200**, 57 (1999).

[5] S. Wolf, D. Awschalom, R. Buhrman, J. Daughton, S. von Molnar, M. Roukes, Y. Chtchelkanova, and D. Treger, Science **294**, 1488 (2001).

[6] J. Slonczewski, J. Magn. Magn. Mater. **159**, L1 (1996); **247**, 324 (2002).

[7] R. Wang *et al.*, Nature (London) **439**, 303 (2006).

[8] A. Imre, G. Csaba, L. Ji, A. Orlov, G. Bernstein, and W. Porod, Science **311**, 205 (2006).

[9] J. Moritz, S. Landis, J. Toussaint, P. Bayle-Guillemaud, B. Rodmacq, G. Casali, A. Lebib, Y. Chen, J. Nozières, and B. Diény, IEEE Trans. Magn. **38**, 1731 (2002).

[10] M. Fitzsimmons *et al.*, J. Magn. Magn. Mater. **271**, 103 (2004).

[11] J. F. Ankner and G. P. Felcher, J. Magn. Magn. Mater. **200**, 741 (1999).

[12] J. P. Hannon, G. T. Trammell, M. Blume, and D. Gibbs, Phys. Rev. Lett. **61**, 1245 (1988).

[13] J. F. MacKay, C. Teichert, D. E. Savage, and M. G. Lagally, Phys. Rev. Lett. **77**, 3925 (1996).

[14] J. W. Freeland, V. Chakarian, K. Bussmann, Y. U. Idzerda, H. Wende, and C. C. Kao, J. Appl. Phys. **83**, 6290 (1998).

[15] R. M. Osgood III, S. K. Sinha, J. W. Freeland, Y. U. Idzerda, and S. D. Bader, J. Magn. Magn. Mater. **199**, 698 (1999).

[16] R. M. Osgood III, S. K. Sinha, J. W. Freeland, Y. U. Idzerda, and S. D. Bader, J. Appl. Phys. **85**, 4619 (1999).

[17] Y. U. Idzerda, V. Chakarian, and J. W. Freeland, Phys. Rev. Lett. **82**, 1562 (1999).

[18] S. Langridge, J. Schmalian, C. H. Marrows, D. T. Dekadjevi, and B. J. Hickey, Phys. Rev. Lett. **85**, 4964 (2000).

[19] A. Scholl, H. Ohldag, F. Nolting, J. Stöhr, and H. Padmore, Rev. Sci. Instrum. **73**, 1362 (2002).

[20] C. H. Marrows, S. Langridge, and B. J. Hickey, Phys. Rev. B **62**, 11340 (2000).

[21] T. P. A. Hase, J. D. R. Buchanan, B. K. Tanner, S. Langridge, R. M. Dalgliesh, S. Foster, C. H. Marrows, and B. J. Hickey, J. Appl. Phys. **93**, 6510 (2003).

[22] V. Ng, Y. V. Lee, B. T. Chen, and A. O. Adeyeye, Nanotechnology **13**, 554 (2002).

[23] M. Albrecht, G. Hu, I. Guhr, T. Ulbrich, J. Boneberg, P. Leiderer, and G. Schatz, Nat. Mater. **4**, 203 (2005).

[24] E. E. Fullerton and S. D. Bader, Phys. Rev. B **53**, 5112 (1996).

[25] J. C. Slonczewski, Phys. Rev. Lett. **67**, 3172 (1991).

[26] R. Felici, J. Penfold, R. C. Ward, and W. G. Williams, Appl. Phys. A: Solids Surf. **45**, 169 (1988).

[27] Y. Yoneda, Phys. Rev. **131**, 2010 (1963).

[28] S. K. Sinha, in *Neutron Scattering in Materials Science*, edited by D. A. Neumann, T. P. Russell, and B. J. Wuensch, MRS Symposia Proceedings No. 376 (Material Research Society, Pittsburgh, 1995), p. 175.

[29] S. K. Sinha, E. B. Sirota, S. Garoff, and H. B. Stanley, Phys. Rev. B **38**, 2297 (1988).

[30] Note that within the Gaussian approximation we treat ϕ as an unrestricted variable, while it is physically restricted to $\pm\pi$. This means that we cannot rigorously treat a system with a totally random distribution of domain directions. Nevertheless, there are many cases where this does not occur in practice, and we expect our formalism to be valid in all cases where there is a specular part in the scattering function. In those cases where σ approaches 2π in width we must take the value derived from fitting to the data *cum grano salis*.

[31] D. R. Lee, S. K. Sinha, C. S. Nelson, J. C. Lang, C. T. Venkataraman, G. Srajer, and R. M. Osgood III, Phys. Rev. B **68**, 224410 (2003).

[32] The experimental geometry was offset to give the largest accessible range of in-plane momentum transfer.

[33] M. Donahue and D. Porter (unpublished).

[34] For the idealized system a perfect array was created in a 2-μm square box. The saturation magnetization and exchange stiffness were 1.422 MA m^{-1} and 30 pJ m^{-1}, respectively.

[35] E. E. Fullerton, D. T. Margulies, M. E. Schabes, M. Carey, B. Gurney, A. Moser, M. Best, G. Zeltzer, K. Rubin, and H. Rosen, Appl. Phys. Lett. **77**, 3806 (2000).

[36] D. R. Lee, G. Srajer, M. R. Fitzsimmons, V. Metlushko, and S. K. Sinha, Appl. Phys. Lett. **82**, 82 (2003).

[37] J. W. Freeland, K. Bussmann, Y. U. Idzerda, and C. C. Kao, Phys. Rev. B **60**, R9923 (1999).

[38] M. Takeda, Y. Endoh, A. Kamijo, and J. Mizuki, Physica B **248**, 14 (1998).

[39] C. H. Marrows, N. Wiser, B. J. Hickey, T. P. A. Hase, and B. K. Tanner, J. Phys.: Condens. Matter **11**, 81 (1999).